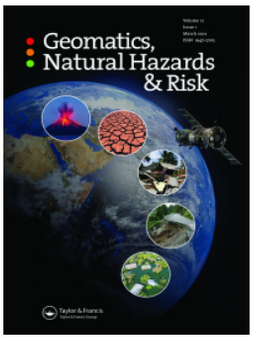

Geomatics, Natural Hazards and Risk

ISSN: (Print) (Online) Journal homepage: www.tandfonline.com/journals/tgnh20

Exploring the relationship between drought-flood abrupt alternation and soil erosion over Guangdong, China through a convection-permitting model

Xuerou Weng, Jinxin Zhu, Dagang Wang, Huijiao Chen, Shuo Wang & Yamin Qing

To cite this article: Xuerou Weng, Jinxin Zhu, Dagang Wang, Huijiao Chen, Shuo Wang & Yamin Qing (2024) Exploring the relationship between drought-flood abrupt alternation and soil erosion over Guangdong, China through a convection-permitting model, Geomatics, Natural Hazards and Risk, 15:1, 2383779, DOI: 10.1080/19475705.2024.2383779

To link to this article: https://doi.org/10.1080/19475705.2024.2383779

GEOMATICS, NATURAL HAZARDS AND RISK
2024, VOL. 15, NO. 1, 2383779
https://doi.org/10.1080/19475705.2024.2383779

Exploring the relationship between drought-flood abrupt alternation and soil erosion over Guangdong, China through a convection-permitting model

Xuerou Weng[a], Jinxin Zhu[a], Dagang Wang[a], Huijiao Chen[b], Shuo Wang[b] and Yamin Qing[b]

[a]Carbon-Water Research Station in Karst Regions of Northern Guangdong, School of Geography and Planning, Sun Yat-Sen University, Guangzhou, China; [b]Department of Land Surveying and Geo-Informatics, The Hong Kong Polytechnic University, Hong Kong, China

ABSTRACT

Climate change has caused a more heterogeneous distribution of extreme precipitation, leading to the deterioration of drought-flood abrupt alternation (DFAA) events and soil erosion. The security and sustainable utilization of water and soil resources are severely threatened. Previous studies have focused separately on these two aspects, failing to comprehensively consider their interrelationship. Furthermore, these studies often rely on climate models with convection parameterization, resulting in substantial uncertainties. We use a 4 km convective permitting model (CPM) to generate reliable outputs for extreme precipitation. By incorporating the long-cycle drought-flood abrupt transition index and the Revised Universal Soil Loss Equation model, we analyze the changes in DFAA events and soil erosion, as well as their interconnectedness. The results show that the CPM outperforms coarse-resolution climate models in reproducing erosive rainfall and simulating the heterogeneous distribution of rainfall by capturing convection processes effectively. Projections indicate an escalation in the occurrence of DFAA events and soil erosion due to the more uneven distribution of precipitation. Specifically, the frequency of flood-to-drought (FTD) events within DFAA is projected to rise from 3.8 to 4.7 per decade. Soil loss is projected to increase 61 $t \cdot hm^{-2} \cdot a^{-1}$, with 73% of the area experiencing more severe soil erosion intensity. A positive correlation between FTD events and soil erosion is found throughout most of Guangdong. This correlation will be further amplified with an increase in the frequency of FTD events. Consequently, existing soil conservation measures are rendered inadequate, presenting substantial challenges for climate change adaptation and ecological protection in the region.

ARTICLE HISTORY
Received 20 February 2024
Accepted 18 July 2024

KEYWORDS
Climate Change; Soil Erosion; Convection Permitting; Drought-Flood Abrupt Alternation

CONTACT Jinxin Zhu zhujx29@mail.sysu.edu.cn

Supplemental data for this article can be accessed online at https://doi.org/10.1080/19475705.2024.2383779.

1. Introduction

The rise in greenhouse gas concentrations in the atmosphere since the Industrial Revolution has contributed to a large rise in the global average temperature, a trend that is expected to continue (IPCC 2021). Due to the atmosphere's improved ability to hold moisture, this warming has intensified the hydrological cycle, resulting in an increase in intense precipitation events (Polade et al. 2017; Wang et al. 2022). Extreme precipitation has already increased globally over the past few decades, according to long-term observations (Papalexiou and Montanari 2019), and future increases are projected by climate models (Pfahl et al. 2017). These climate changes raise concerns about processes driven by large-scale precipitation events, such as intensified soil erosion and the growing occurrence of compound extreme climate events in the future (Borrelli et al. 2020; Azari et al. 2021; Chen and Wang 2022; Chen et al. 2023). Soil erosion and compound extreme climate events are interconnected and represent significant ecological and environmental issues. Frequent natural disasters, including floods and droughts, exacerbate soil erosion, while severe soil erosion negatively impacts the ecological environment, further contributing to droughts and floods (Zhang et al. 2016; Shmilovitz et al. 2021; Masroor et al. 2022). The direct causal relationship between soil erosion and droughts or floods is well-established (Li and Fang 2016; Masroor et al. 2022). Uncertainty persists, especially in light of global warming, regarding the connection between several extreme events, such as droughts and floods, and their effects on soil erosion. Moreover, while global climate models (GCMs) and regional climate models (RCMs) are commonly used in climate change impact studies, the potential added value of employing higher resolution climate models, such as the 4 km convection-permitting models (CPMs), for precipitation simulations is still to be explored.

Soil erosion, aggravated by climate change, poses a critical environmental challenge with wide-ranging implications for global food security (Jaafari et al. 2022; Basheer et al. 2024). This process predominantly affects the vital topsoil layer, resulting in diminished soil fertility and potential food shortages (Schulze and Freibauer 2005; Amundson et al. 2015; Borrelli et al. 2017). Global evidence already indicates the influence of climate change on soil erosion patterns (Li and Fang 2016), and projections suggest a staggering 30% to 66% increase in global soil erosion due to shifts in the hydrological cycle (Borrelli et al. 2020). Through modifications in rainfall intensity and distribution, studies have examined how climate change affects soil erosion (Nearing et al. 2004; Azari et al. 2021). Furthermore, the interplay of warmer temperatures and seasonal droughts, linked to climate change, alters vegetation coverage and soil moisture, indirectly influencing soil erosion processes (Masroor et al. 2022). With mounting concerns about environmental sustainability and food security, various models have been developed to assess the precise impact of climate change, particularly precipitation-induced floods and droughts, on global soil erosion. Among these models, the Revised Universal Soil Loss Equation (RUSLE) has emerged as a widely employed and crucial tool for formulating effective environmental and agricultural policies and strategies aimed at managing soil erosion and mitigating potential threats to human well-being (Ganasri and Ramesh 2016; Borrelli et al. 2020). Compared with the physical erosion model, the RUSLE model has obvious advantages in terms of

computing resource requirements, ease of use, and universality. In addition, this study mainly focuses on the soil erosion caused by rainfall, rather than the loss described by complex physical models. When using a physical model to simulate the runoff process, detailed parameter settings and input of physical quantities are usually required, and the error superposition of these parameters and input quantities may cause great uncertainty in the results. Therefore, the RUSLE model is more in line with the actual needs of this study and can more accurately assess the impact of extreme rainfall on soil erosion.

The growth and severity of extreme climate events have become an important challenge to the stability of both global and regional natural settings against the backdrop of global warming (AghaKouchak et al. 2014; Horton et al. 2015; Zscheischler and Seneviratne 2017; Guo et al. 2023). These events, often not isolated occurrences, stem from the complex interplay and temporal-spatial coupling of multiple factors, forming compound events (Zscheischler et al. 2020; Zhang et al. 2021a; Chen et al. 2023). Research has highlighted the substantial amplification of negative impacts associated with compound extreme climate events, leading to heightened ecological and socio-economic hazards compared to individual extremes (AghaKouchak et al. 2020; Weber et al. 2020; He et al. 2022). Drought-flood abrupt alternation (DFAA) events are one of the most notable types of compound climate events that have drawn increased attention (Chen and Wang 2022; Qiao et al. 2022; Chen et al. 2023). Drought-to-flood (DTF) and flood-to-drought (FTD) events are examples of DFAA events that quickly change from one state of drought or flood to the other within short durations. These phenomena frequently cause more catastrophic disasters than isolated drought or flood events (Yu et al. 2019; Zhu et al. 2020; Bi et al. 2022). Earlier research has demonstrated that DFAA occurrences are becoming more frequent and intense, along with an expanding regional spread (Ma et al. 2019; Chen et al. 2020; Zhang et al. 2023). Thus, understanding the evolution of extreme DFAA events holds significant value for flood and drought disaster warning and mitigation efforts in changing environments. Furthermore, the compounded effects of climate-change-exacerbated droughts, floods, and soil erosion present multifaceted environmental, economic, and social challenges globally. However, limited research has focused on the complex relationship between several extreme events and soil erosion, impeding the creation of efficient solutions for coping with and adapting to climate change.

Precipitation anomalies play a dominant role in the occurrence of DFAA events and the intensification of soil erosion. However, the majority of climate models still face significant difficulties in effectively reproducing precipitation (Qiao and Liang 2015). Increasing model resolution is a common approach to improve precipitation simulations, as it enables a more realistic representation of dynamic and physical processes in climate models (Gao et al. 2006). Studies have repeatedly demonstrated that models performed at a finer scale are more accurate in capturing the severity, frequency, and spatiotemporal variability of extreme events and climate variables (Lucas-Picher et al. 2017; Shu et al. 2022; Ascott et al. 2023). CPMs with resolutions less than 4 km have drawn interest recently because of their capacity to deliver more dependable fine-scale climate information. CPMs are also capable of simulating the

interaction between large-scale changes in atmospheric circulation and local-scale processes complicated by terrain (Prein et al. 2015; Guo et al. 2019). Convection parameterization, a significant source of errors and uncertainties in RCMs, is not a factor in CPMs (Dai et al. 1999; Ban et al. 2014). The superiority of CPMs over RCMs in replicating mean precipitation, regional patterns, and extremes has been shown in studies (Chan et al. 2014; Fosser et al. 2015; Liu et al. 2023). However, it is necessary to further examine the capability of CPMs in simulating compound extreme events and their impacts on soil erosion.

Therefore, the RUSLE and CPM models are combined with an empirical technique of sudden drought-flood alternation in order to answer the following research questions: (1) How does transitioning from a 25 km (RCM) to a 4 km (CPM) grid size impact future soil erosion and DFAA events? (2) What is the spatial correlation between soil erosion and DFAA events, and how will their interaction evolve under the influence of climate change?

2. Data and methods

2.1. Study area

Guangdong Province has had a rapid convergence of economy, population, and resources in recent decades as a result of its significance as a major engine of China's economic expansion, amplifying the effects of climate change (Li et al. 2020). Therefore, it is of great scientific and practical importance to perform a thorough assessment of the state and dynamics of Guangdong's water and soil resources. Guangdong province, which spans an area of $17.98 \times 10^4\,km^2$, is situated along China's southeast coast at 20°13′ ∼25°31′ N,109°39′ ∼117° 19′ E. The province experiences typical subtropical monsoon weather and is very susceptible to typhoons, droughts, and floods. The typical annual temperature is 18 °C–24 °C, and there is a lot of rainfall on a yearly average of about 1,700 mm. However, the amount of precipitation varies throughout the year, with more than 80% of it falling between April and September. The province's geological structure is complex with granite, sand shale, metamorphic rock, limestone, red rock series, and other rocks widespread in the middle and low mountains, hills, and basins. Among them, granite and sand shale are the most developed and prone to weathering and soil erosion, especially under hot and rainy conditions.

2.2. Data

The CPM used in the study is based on the Weather Research and Forecasting Model (WRF) for Guangdong Province and its surrounding areas. A two-way triple nesting setup is used in the model experiment design, which covers the simulation for a historical (1980–2005) period and the projection for a future (2074–2099) period. As illustrated in Figure 1, simulations for the outer two domains (D01 and D02) use parameterized convection mode while convection-permitting mode for the inner domain (D03). With 78×66 grid points and a 35 km resolution, the domain D01 covers a significant portion of South China. The domain D02 is resolved with 144×108 grid

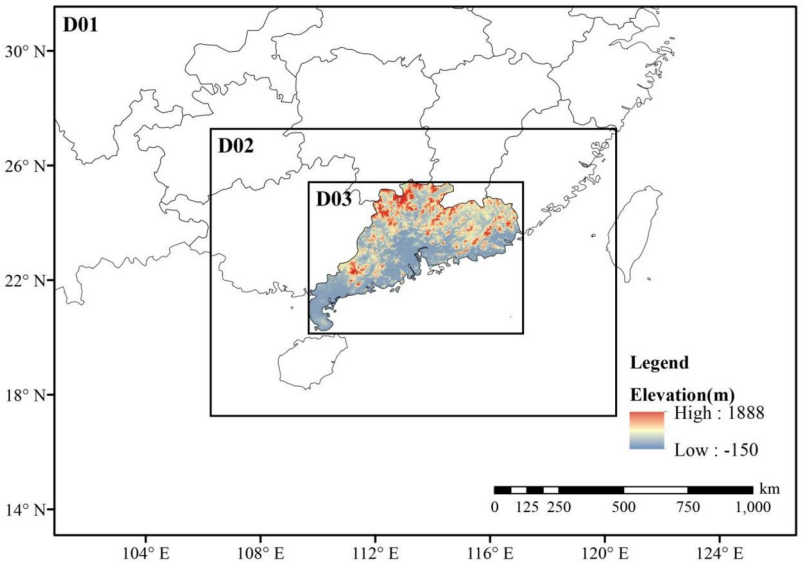

Figure 1. The triple nesting illustration and geographical location of the study area.

points and 10 km grid spacing. The Guangdong Province is covered by the domain D03, which has a 4 km grid spacing (212 × 168 grid points). The ERA-Interim reanalysis product, which features updates every 6 h and a resolution of 75 × 75 km, is used to determine the initial and lateral boundary conditions, as well as force the climate projection for the future period. Using a multi-model ensemble mean climate change signal, a pseudo-global warming (PGW) technique is utilized to successively alter the initial and boundary conditions. The climate perturbation is estimated using the outputs of the Coupled Model Intercomparison Project Phase 5 (CMIP5) GCMs under the Representative Concentration Pathways 8.5 (RCP8.5). We employ a multi-model ensemble mean climate difference between the present simulation and the future projection to explore the model uncertainty. In the ensemble, ten CMIP5 GCMs are chosen depending on how well they reproduce the climate over China, including GFDL-CM3, HadGEM2-CC, HadGEM2-ES, CMCC-CM, MRI-CGM3, IPSL-CM5A-LR, CSIRO-Mk3.6.0, CanESM2, MIROC-ESM, and MRI-CGCM3.

To evaluate the performance of CPM simulation in producing precipitation over Guangdong Province, we utilize the 1 km monthly precipitation dataset for China (1901–2021) compiled by Peng (2020) as our observational dataset. Based on the worldwide high-resolution climate dataset provided by WorldClim and the global 50 km resolution climate dataset published by the Climatic Research Unit (CRU), the dataset was created via the Delta downscaling procedure in the Chinese region. Moreover, data from 496 meteorological stations are used to further validate the results with credibility (Peng et al. 2019). We selected five RCMs (CCLM, HCLM, MCLM, IDMI, PREC) from the Coordinated Regional Climate Downscaling Experiment (CORDEX) to compare with the CPM in terms of the skill in reproducing historical precipitation. These RCMs use a cumulus convective parameterization scheme to deal with the physical process of atmospheric non-adiabatic heating.

Additional details regarding the soil, terrain, vegetation, and land-use characteristics are presented in Table S1.

2.3. RUSLE model

The RUSLE approach has been frequently used to predict soil erosion and estimate annual soil loss utilizing separate parameters. The soil erosion per unit area is given by the RUSLE equation and is denoted as Bi et al. (2023):

$$A = R \times LS \times K \times C \times P \tag{1}$$

Where A is the annual soil erosion ($t{\cdot}hm^{-2}{\cdot}a^{-1}$); R is the rainfall erosivity factor ($MJ{\cdot}mm{\cdot}hm^{-2}{\cdot}h^{-1}{\cdot}a^{-1}$); K is the soil erodibility factor ($t{\cdot}hm^{2}{\cdot}h{\cdot}MJ^{-1}{\cdot}hm^{-2}{\cdot}mm^{-1}$); C is the cover management factor; LS is the slope length-steepness factor; P is the conservation support practice factor.

2.3.1. Rainfall erosivity factor (R)

The *R*-factor describes how easily rains and the resulting runoff can separate and move soil particles. The complexity of the calculation procedure and the difficulty of data collecting have led to the development of a number of models that use diverse rainfall data to determine rainfall erosivity. Zhang et al. (2021b) evaluated a number of straightforward methods developed for determining rainfall erosivity over mainland China and found that, due to its straightforward formula, the Xie model (Xie et al. 2016) is more accurate. This model was also adopted in the Chinese Soil Loss Equation and the First National Water and Soil Conservation Survey (Liu et al. 2020). The formula is expressed as:

$$R_d = \alpha P_d^{1.7265} \tag{2}$$

where R_d is the daily rainfall erosivity, $MJ{\cdot}mm{\cdot}hm^{-2}{\cdot}h^{-1}$; L is the day in the half-month; P_d is the effective rainfall for day d, by which P_d is set to the actual value of a rainfall event when its value is over 10 mm/day, otherwise, P_j is set to zero; α are parameters. α is 0.3937 in the warm season (May to September) and 0.3101 in the cold season (October to April).

2.3.2. Soil erodibility factor (K)

The *K*-factor reflects the susceptibility of the soil to erosive power stripping and transport. The higher the K value, the weaker the erosion resistance of the soil. Equation (3) developed by Williams (1990) is used to compute the *K*-factor.

$$\begin{aligned} K = {} & \left\{0.2 + 0.3\exp\left[-0.0256 m_s(1 - m_{silt}/100)\right]\right\} \times \left[m_{silt}/(m_c + m_{silt})\right]^{0.3} \\ & \times \left\{1 - 0.25 orgC/[orgC + \exp(3.72 - 2.95 orgC)]\right\} \\ & \times \left\{1 - 0.7(1 - m_s/100)/\left\{(1 - m_s/100) + \exp\left[-5.51 + 22.9(1 - m_s/100)\right]\right\}\right\} \end{aligned} \tag{3}$$

Where m_s, m_{silt}, m_c, $orgC$ are the percentage content of sand, silt, clay, and organic matter, respectively. The calculated K value needs to be multiplied by 0.1317 to convert to the International System of Units.

2.3.3. Slope length-steepness factor (LS)

The LS factor illustrates how slope steepness and length affect soil erosion. The digital elevation model (DEM) of the study area is geometrically rectified and retrieved using ArcGIS to ascertain the LS factor. The LS-factor is determined by Equation (4)–(7) (Phinzi and Ngetar 2019; Elnashar et al. 2021).

$$L = (\lambda/22.13)^m \tag{4}$$

$$m = n/(n+1) \tag{5}$$

$$n = (\sin\theta/0.0896)/(3\sin^{0.8}\theta + 0.56) \tag{6}$$

$$S = \begin{cases} 10.8\sin\theta + 0.03 & (\theta < 5^\circ) \\ 16.8\sin\theta - 0.05 & (5^\circ \le \theta < 10^\circ) \\ 21.9\sin\theta - 0.96 & (\theta \ge 10^\circ) \end{cases} \tag{7}$$

where λ is the horizontal slope length; the exponent m is related to the ratio of rill to inter-rill erosion (n); θ is the slope angle in degree.

2.3.4. Cover management factor (C)

The C-factor is a non-dimensional term that describes the ratio of soil loss from land that has been cultivated under specific conditions to the matching clean-tilled continuous fallow. Its value ranges from 0 to 1, with higher values indicating weaker erosion inhibition (Thomas et al. 2018; Tian et al. 2021). Currently, the normalized vegetation index (NDVI) is commonly employed to estimate the C-factor. The C-factor is computed using the following equation (Thomas et al. 2018):

$$C = \exp\left(-\alpha\frac{NDVI}{\beta - NDVI}\right) \tag{8}$$

where α and β are the parameters defining the shape of the NDVI-C curve, and an α value of 2 and a β value of 1 provide reasonable results (Knijff et al. 2000).

2.3.5. Conservation support practice factor (P)

The P-value is a dimensionless variable with a range of 0 to 1, with a value of 0 or almost zero suggesting more successful conservation practices for reducing soil erosion and vice versa. Values for P have the worst reliability of all the erosion factors. Previous research has shown that the P values can be precisely specified based on the various forms of land use (Tang et al. 2015; Xue et al. 2018; Ghosal and Das Bhattacharya 2020). With the kind of land use, the P factor's spatial distribution varies. The dataset of land use types adopted in this article includes the land use

categories of paddy fields, dry land, forest land, grassland, water area, urban land, and unutilized land. In this study, the *P*-values of these 7 types were defined as 0.05, 0.4, 1, 1, 0, 0.3, and 1, respectively.

2.4. Determination of drought-flood abrupt alternation

The long-cycle drought-flood abrupt transition index (LDFAI) proposed by Wu et al. (2006) has been utilized across the majority of China's regions to assess the sudden change between drought and flood events (Liu et al. 2019; Cai et al. 2020; Shi et al. 2021; Ren et al. 2023), including two case studies for Guangdong Province (He et al. 2016; Li et al. 2021). The calculation details are shown as follows:

$$\mathrm{LDFAI} = (R_j - R_i) \times \left(|R_i| + |R_j|\right) \times 1.8^{-|R_i+R_j|} \tag{9}$$

where R_i and R_j represent the standardized precipitation in the pre-flood and post-flood periods, respectively. $(R_j - R_i)$ denotes the intensity of DFAA events, while $(|R_i|+|R_j|)$ represents combined intensity of the drought and flood. The weight coefficient $1.8^{-|Ri+Rj|}$ reduces the weight of pure drought or flood events and increases the weight of DFAA events. It is important to note that LDFAI values greater than 1 indicate drought-to-flood (DTF) events, while values less than −1 represent flood-to-drought (FTD) events. FTD events occur when excessive rainfall leads to surface water accumulation, followed by a decrease or cessation of rainfall, resulting in rapid surface water disappearance and soil drying. DTF events refer to sudden heavy rain or flooding after a prolonged dry period, resulting in an instant increase in surface water. The magnitude of the LDFAI value indicates the severity of the drought-flood abrupt alternation events, with larger absolute values indicating greater severity. To determine the time scale for the LDFAI method, we focused on the pre-flood and post-flood seasons in Guangdong Province. The pre-flood period encompasses April through June, while the post-flood period spans July through September (He et al. 2016). These time intervals are selected based on the hydrological and meteorological characteristics associated with monsoons and cyclones in the study area. During the post-flood period, the activity of typhoons and the intertropical convergence zone plays a significant role in shaping summer precipitation patterns. On the other hand, the pre-flood season experiences high activity from systems such as fronts, upper troughs, and the southwest monsoon. These two systems are the main influencing factors for precipitation distribution in Guangdong Province.

2.5. Generalized extreme value distribution

The Generalized Extreme Value (GEV) distribution is introduced to characterize the distribution of extreme precipitation and to explore the change in the probability of future risk of extreme precipitation from the perspective of a probability distribution (Coles 2001). The probability distribution function is:

$$F(x;\mu,\sigma,\xi)=\begin{cases}\exp\left[-\exp\left\{-\dfrac{x-\mu}{\sigma}\right\}\right], \xi=0\\ \exp\left[-\left\{1+\xi\frac{x-\mu}{\sigma}\right\}^{-\frac{1}{\xi}}\right], \xi\neq 0, 1+\xi\dfrac{x-\mu}{\sigma}>0\end{cases} \tag{10}$$

where μ, σ, and ξ are location, scale, and shape parameters, respectively. The value of the shape parameter ξ is the key to determining the type of extreme value distribution. When $\xi=0$, the distribution is Gumbel; when $\xi<0$, it is Weibull distribution; when $\xi>0$, it is Fréchet distribution. The method of maximum likelihood estimation is employed to obtain estimates of the above three parameters, as it is considered more robust than traditional moment estimation.

3. Results

3.1. Validation of rainfall data

We evaluated the accuracy of soil erosion simulations by gauging the skill of models in reproducing erosive rainfall. Figure 2 shows the domain-averaged daily erosive rainfall from 4 km CPM and 25 km RCMs against the observed data. It can be seen that all RCMs have a dry bias, with the simulated erosive rainfall 1.5–2.1 mm/day lower than the observed data. The MCLM model with 2.1 mm/day has the largest dry bias among all RCMs. All RCMs have a consistent spatial pattern for the dry bias which is located in the central part of the study area. The CPM with a 0.9 mm/day dry bias demonstrates a better performance than RCMs. The erosive rainfall simulated by the CPM has a mixed pattern of biases, with dry biases in the northeast and wet biases in the southwest. Convective parameterization has been found to have the potential to cause simulation errors, including inaccurate depictions of the daily cycle's beginning and peak, an overestimation of the frequency of low precipitation

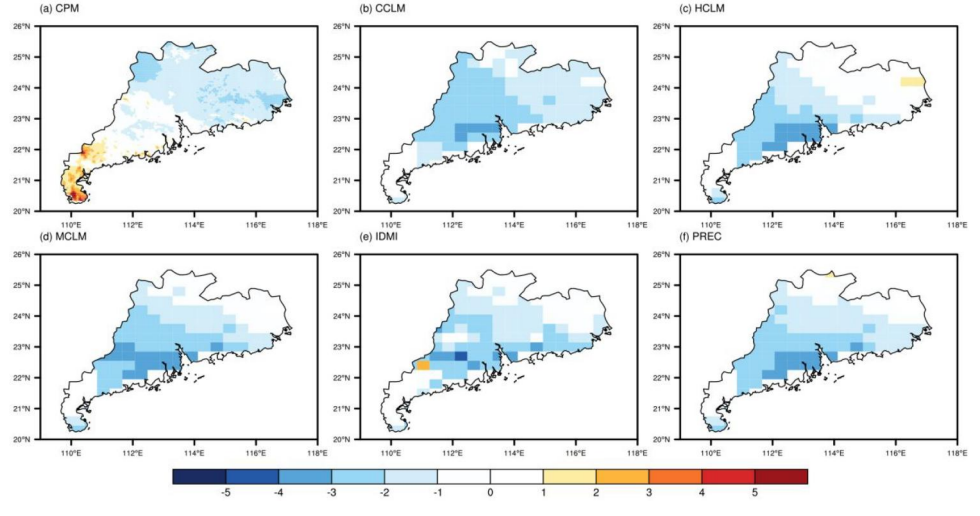

Figure 2. Spatial distributions of erosive rainfall (>10 mm/day) biases between observation and simulations derived from the CPM and five RCMs (units: mm/day).

intensity events, and an underestimation of hourly precipitation intensity (Dai et al. 1999; Ban et al. 2014). The CPM with the ultra-high resolution is able to resolve the convection process and provides fine-scale forcing information for complex topography. Furthermore, the CPM has a relatively high capability in capturing short-lived extreme events (Chan et al. 2014; Fosser et al. 2015; Liu et al. 2023). Based on the distribution of rainfall contours in the study region produced from the measured rainfall data (Liao et al. 2014), the CPM performs better than RCMs at capturing the occurrence of erosive rainfall with high values over the study area. Extreme rainfall events are anticipated to increase in frequency and severity relative to normal conditions in the context of rapid global climate change. Reliable identification of heavy rainfall is necessary for soil erosion studies.

The distribution of extreme precipitation is commonly assumed to follow the GEV distribution (Ban et al. 2020). We calculate the probability density function (PDF) and cumulative density function (CDF) using the extreme precipitation indices to fit the GEV distribution, using the monthly maximum precipitation across all grids. Figure 3 displays the PDF and CDF distributions of the CPM and ensemble-mean RCMs for both historical and future periods. The fitted PDF of the CPM exhibits larger scale and shape parameters compared to the RCMs, indicating a more heterogeneous precipitation distribution. Notably, the probability of no precipitation increases approximately tenfold. Additionally, the cumulative probability of rainfall intensities ranging from 0 to 20 mm/day decreases from 0.94 to 0.51. Moreover, the CPM projects a maximum rainfall intensity of 110 mm/day, surpassing the 40 mm/day estimated by RCMs. Consequently, the CPM model captures a more diverse precipitation probability distribution than the RCMs. The probabilities of no rainfall events and extreme precipitation events significantly increase, while the occurrence probability of daily precipitation ranging from 0 to 20 mm greatly reduces. Furthermore, the CPM demonstrates the ability to simulate precipitation intensities

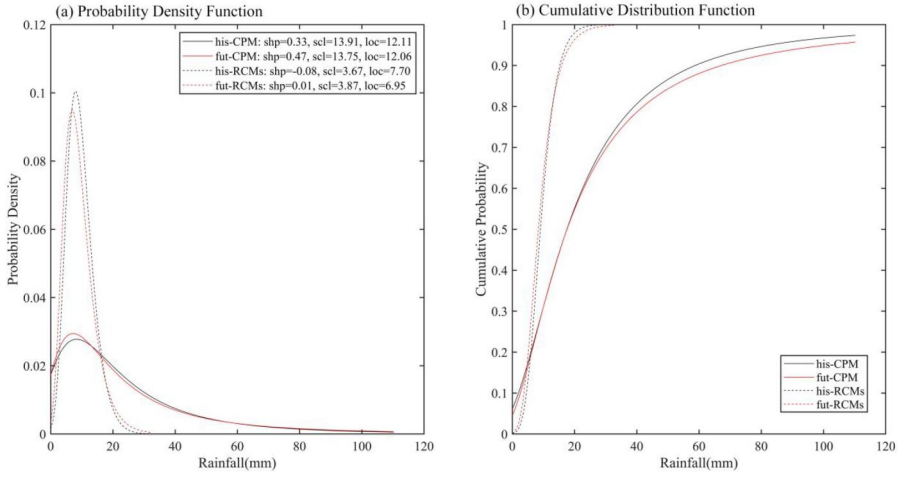

Figure 3. PDF (a) and CDF (b) distributions for the CPM and RCMs ensemble (black and red curves denote historical and future periods; solid and dashed lines denote the CPM and RCMs results; shp for the shape parameter; scl for the scale parameter; loc for the position parameter).

not observed in RCMs. Under warming conditions, the shape, position, and scale parameters of the PDF curves exhibit certain variations. The CPM results show an increase in the shape parameter, while the other two parameters decrease for the future relative to the historical period. As the position parameter decreases, the corresponding probability density curve shifts to the left. The scaling parameter reduces from 13.91 to 13.75, resulting in a narrower probability density curve. Overall, the distribution of precipitation is expected to become more heterogeneous in the future period compared to the historical period.

Climate change amplifies the hydrological cycle, resulting in greater temporal and spatial variations in precipitation. As a consequence, there is an increased occurrence of contrasting dry and wet periods, with more frequent abrupt alternations between drought and flood events (the term 'DFAA'). LDFAI is commonly employed for quantitative analysis of DFAA events, capturing their fundamental characteristics. LDFAI values greater than 1 signify drought-to-flood events, while values less than −1 indicate flood-to-drought events. To assess the model's performance in simulating DFAA events, we compare the absolute difference between the observed and simulated LDFAI values (Figure 4). On one hand, the results of the RCMs against the observation vary among the models utilized in this study. The MCLM model closely approximated the observed LDFAI value, differing by only 0.04. However, the simulations generated by the CCLM, HCLM, and PREC models exhibited higher LDFAI values than the observed data in most areas, with differences ranging from 0.27 to 1.31. This indicates that these RCMs tend to simulate more DTF events than FTD events within the DFAA events, particularly in the southern part of the region. Conversely, the IDMI model yielded an LDFAI value of 0.32 lower than the observed result. On the other hand, the CPM model tended to simulate more FTD events rather than DTF events, showing a difference of 0.67 compared to the observed result. This suggests that the CPM model is more effective in capturing extreme rainfall events during the April–June period. It is worth noting that this phenomenon

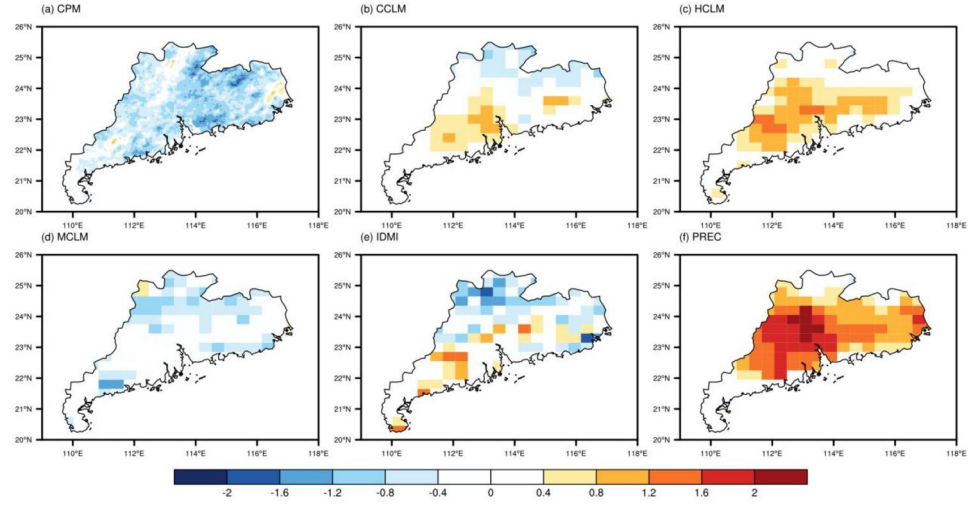

Figure 4. Spatial distributions of LDFAI biases between observation and simulations derived from the CPM and five RCMs.

may be attributed to the convective permitting scale of the CPM, which could potentially overestimate rainfall extremes by emphasizing deep convective processes.

Determining the occurrence of DFAA events in the study area by using the LDFAI values is essentially an evaluation of the temporal distribution of rainfall during the flood season period (April-September). In order to gain a deeper understanding of the characteristics of the occurrence of DFAA events in the study area, the intra-annual variability of rainfall obtained from the model simulations is further analyzed (Figure 5). As can be seen from Figure 5, the intra-annual variability of rainfall in the study area shows a bimodal pattern, with peaks occurring in May to June and August, during which the cumulative rainfall accounts for about 46% of the annual rainfall. The monthly rainfall in the study area simulated by the RCMs is generally low, and the characteristics of the intra-annual variability of rainfall simulated by RCMs are different from each other. This reflects the limitations of the RCMs in modeling the intra-annual variability of rainfall. Looking at the ups and downs of the intra-annual variability curves, it is clear that the CPM is closer to the observed dataset in modeling the monthly rainfall variability during the flood season. Although the simulated results of CPM are also lower than the observed values, CPM shows a clear advantage in capturing the occurrence of monthly rainfall events compared to the coarser resolution RCMs. This implies that CPM is closer to reality in modeling intra-annual variations in rainfall and provides more reliable simulation results for the study.

We have derived statistical results from the erosive rainfall and LDFAI simulations, which are presented in Table 1. The table presents the spatial correlation coefficient (CC), root mean square error (RMSE), and Kling Gupta efficiency (KGE) between the model outputs and observations. A higher CC, a smaller RMSE, and a larger KGE indicate a stronger correlation between the model and the data, indicating better simulation performance. Notably, the CPM demonstrates a greater advantage in simulating erosive rainfall compared to simulating LDFAI. With increasing model resolution, the CCs for simulating erosive rainfall improve from −0.50 for RCMs to 0.54 for CPM, the RMSE decreases from 844.39 to 681.26, and the KGE increases to 0.20. In terms of simulating LDFAI values, the CPM outperforms RCMs with a higher CC of 0.78, a lower RMSE of 0.77, and a larger KGE of −0.79. Based on the spatial

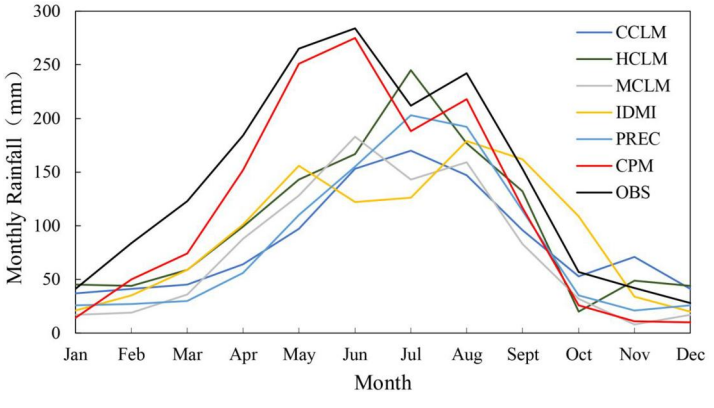

Figure 5. Annual variation curve of rainfall from CPM and RCM simulations.

Table 1. The CC, RMSE, and KGE between observation and simulations in terms of the erosive rainfall and LDFAI.

	Erosive Rainfall			LDFAI		
Models	CC	RMSE	KGE	CC	RMSE	KGE
CCLM	−0.31	944.68	−0.53	0.78	0.49	0.11
HCLM	−0.64	844.39	−2.20	0.68	0.73	−0.84
MCLM	−0.64	1043.6	−2.97	0.71	0.48	−1.80
IDMI	−0.27	905.48	−0.61	0.58	0.7	0.03
PREC	−0.66	998.64	−1.88	0.44	1.38	−2.64
CPM	0.54	681.26	0.20	0.78	0.77	−0.79

Table 2. The proportion of area for different erosion intensity levels in Guangdong Province over two periods.

Levels	Mired erosion	Mild erosion	Moderate erosion	Intensity erosion	Extreme intensity erosion	Violent erosion
1980–2005	90.81%	7.17%	1.08%	0.38%	0.18%	0.39%
2074–2099	90.09%	7.68%	1.21%	0.34%	0.30%	0.39%

distribution analysis and associated statistics, it is evident that CPM provides more accurate simulations than RCMs. Therefore, we will utilize the CPM simulation results to analyze the response of soil erosion to climate warming and its interactive relationship with DFAA events in the study area.

3.2. Soil erosion and DFAA projections

The study reveals that future rainfall increases will lead to elevated soil erosion rates. Among the various factors considered (*K*, *LS*, *C*, and *P*), the model's results are predominantly influenced by changes in the *R*-factor. The changes in soil erosion are projected across Guangdong Province based on the CPM projections (as shown in Figure 6). The findings indicate that the average regional soil erosion rate in Guangdong Province will rise by 26%, from 232 $t{\cdot}hm^{-2}{\cdot}a^{-1}$ in the historical period to 293 $t{\cdot}hm^{-2}{\cdot}a^{-1}$ in the future. Significant increases in soil erosion are expected in the central part of the study region, while the southwestern and northeastern areas are projected to experience a decrease. Approximately 77% of the study area is anticipated to encounter increased soil erosion. In accordance with the soil erosion classification and grading standards (SL190-2007) issued by the Ministry of Water Resources of China in 2008, the calculated soil erosion levels in this study are classified into six categories. These range from mild erosion to violent erosion, with higher levels indicating more severe soil loss. Table 2 presents the proportion of each soil erosion intensity grade in the study area for 1980–2005 and 2074–2099. Currently, the study area primarily experiences mild erosion, accounting for 90% of the total area. However, in the future period, approximately 0.68% of the area is expected to transition from mild erosion to mild, moderate, or extreme intensity erosion. This transition corresponds to an area of approximately 1,283 km^2, which is roughly equivalent to the size of Shenzhen city.

Figure 7 displays the spatial pattern of DTF and FTD frequencies simulated by CPM for the historical and future periods. The number of DFAA events (DTF and

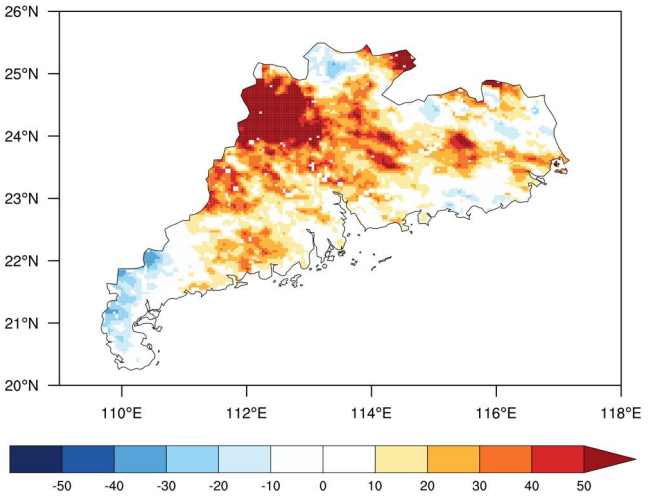

Figure 6. Percentage change of annual soil erosion (unit: %) derived from the CPM for 2074-2099 relative to 1980-2005.

FTD combined) in Guangdong Province has slightly increased under warming conditions. However, the proportion of the two types of events in DFAA will undergo significant changes under the RCP8.5 scenario compared to the historical period. The frequency of FTD events is found to increase from 3.8 to 4.7 per decade in the future, while the frequency of DTF events is projected to decrease from 0.8 to 0.1 per decade. The FTD events have a relatively high proportion in both historical and future periods, but under RCP8.5, the frequency of FTD events further increases, while DTF events decrease significantly. This results in a further rise in the proportion of FTD events in DFAA. In terms of spatial distribution, FTD events are concentrated in the relatively flat areas of western Guangdong and the Greater Bay Area, with fewer occurrences in the mountainous regions of northern Guangdong. Under climate warming, FTD events show an increasing trend in both western Guangdong and the Greater Bay Area, with the most significant increase observed in western Guangdong. Additionally, FTD events expanded towards the northern and eastern parts of Guangdong, leading to a doubling of FTD events in these regions compared to the historical period. DTF events, on the other hand, are mainly concentrated in the mountainous regions of northern Guangdong. With climate warming, the area affected by DTF events significantly decreased and is limited to the northernmost boundaries. The FTD events have a relatively high proportion of DFAA in both periods, indicating that a higher amount of precipitation occurs in the pre-flood season from April to June. The more uneven distribution of precipitation, as mentioned before in the GEV analysis, contributes to the observed temporal shift in DFAA.

To assess changes in the magnitude of FTD and DTF events, we utilized the GEV distribution function to analyze the variations in precipitation during the pre-flood period and post-flood period. The resulting PDFs are depicted in Figure 8 for both historical and future periods. Comparing the scale and location parameters of pre-flood and post-flood precipitation, we observe that heavy rainfall events (>30 mm/day) are more prevalent in the pre-flood period across historical and future periods.

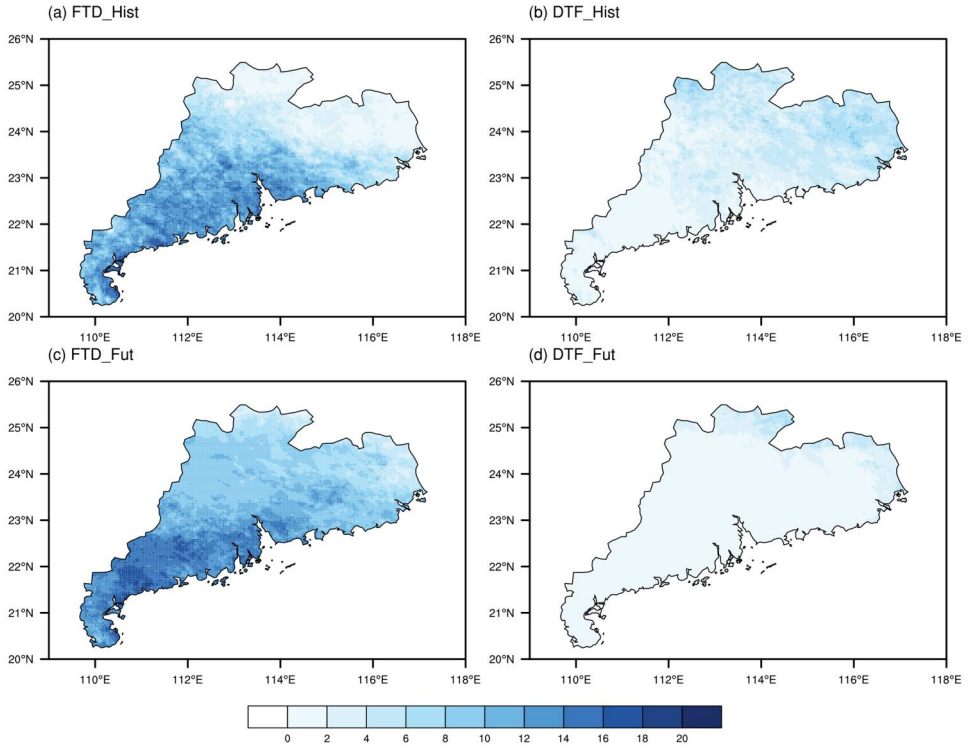

Figure 7. The spatial distribution of DTF and FTD frequencies for historical and future periods.

Climate warming intensifies this discrepancy, as it amplifies the scale and location parameters during the pre-flood period while reducing them in the post-flood period. In the historical period, the probability of a 39 mm/day rainfall event is highest during the pre-flood period, while a 26 mm/day rainfall event corresponds to the peak value of the probability density in the post-flood period. Under RCP8.5, the PDF curve for the pre-flood period becomes shorter and wider, indicating a higher frequency of extreme precipitation events compared to the historical period. For example, the tail distribution of heavy rainfall events (>30 mm/day) under RCP8.5 is nearly three times that of the historical period. Conversely, the fitted curve for the post-flood period becomes taller and narrower, indicating a shift towards drier days. The probability of no precipitation during the post-flood season increases from 7×10^{-4} to 35×10^{-4} under climate change. These findings confirm that the study area is becoming more susceptible to compound extreme events of FTD. Overall, our analysis highlights the changing nature of precipitation patterns and the increased risk of compound extremes in the study area.

3.3. Relationship between soil erosion and DFAA

The impacts of the FTD and DTF events on soil erosion are slightly different. In FTD events, the sudden disappearance of surface water leads to rapid soil surface drying, resulting in hardened soil surfaces. This makes it difficult for rainwater to

penetrate the soil, increasing the risk of soil erosion (Peng et al. 2007; Zhang et al. 2013). In DTF events, the soil texture may become loose and more susceptible to erosion and sedimentation by water flow due to prolonged drought and soil dryness (de Vries et al. 2023; Du et al. 2023). Both FTD and DTF events pose potential risks of soil erosion. Pearson correlation is used to examine the relationship between soil erosion and DFAA events. As shown in Figure 9 , in the historical period, there is a positive correlation between FTD events and soil erosion in the relatively flat areas of western Guangdong and the Greater Bay Area. On the other hand, DTF events are strongly positively correlated with soil erosion in the mountainous regions of northern Guangdong. This is consistent with the spatial distribution of these two events. Some regions with positive correlations with both event types experience the combined influence on soil erosion. It is worth noting that, although FTD events have a higher proportion in the DFAA in western Guangdong and the Greater Bay Area, this does not affect the positive correlation between DTF events and soil erosion in these areas. Specifically, in the Leizhou Peninsula of western Guangdong (21°N, 110°W), there are more FTD events than DTF events, but soil erosion is more strongly associated with DTF events. However, in the future period, the proportion of FTD events further increases, and the proportion of DTF events further decreases. Soil erosion in nearly the entire Guangdong Province shows a positive correlation with FTD events, with the area-averaged correlation coefficient increasing from 0.18 in the historical period to 0.53, nearly tripling. Nearly all of the regions where soil erosion is positively linked with DTF episodes have vanished. In order to accommodate for the changes in extreme occurrences brought on by climate change, the Guangdong Province must update its soil and water conservation policies. It is important to note that under the influence of climate change, the primary event of soil erosion in the mountainous regions of northern Guangdong has shifted from

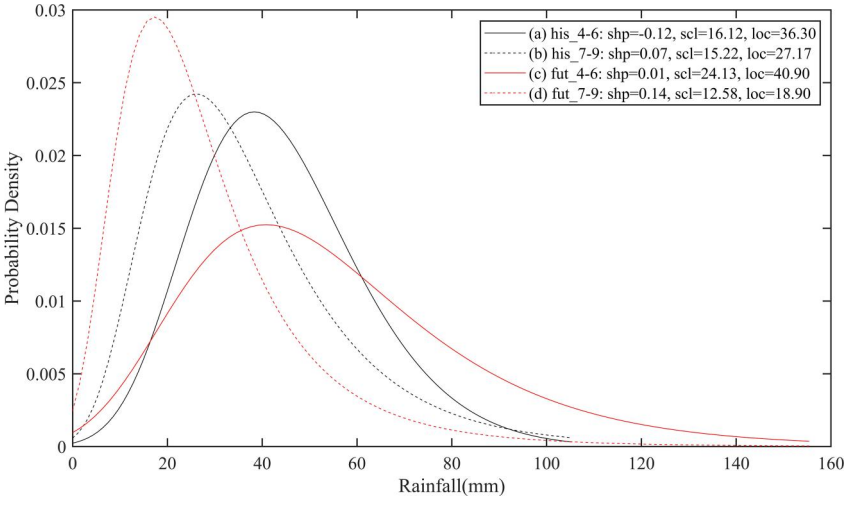

Figure 8. PDF distributions for precipitation derived from the CPM for pre-flood and post-flood periods (black and red curves denote historical and future periods; solid and dashed lines denote pre-flood and post-flood results; shp for the shape parameter; scl for the scale parameter; loc for the position parameter).

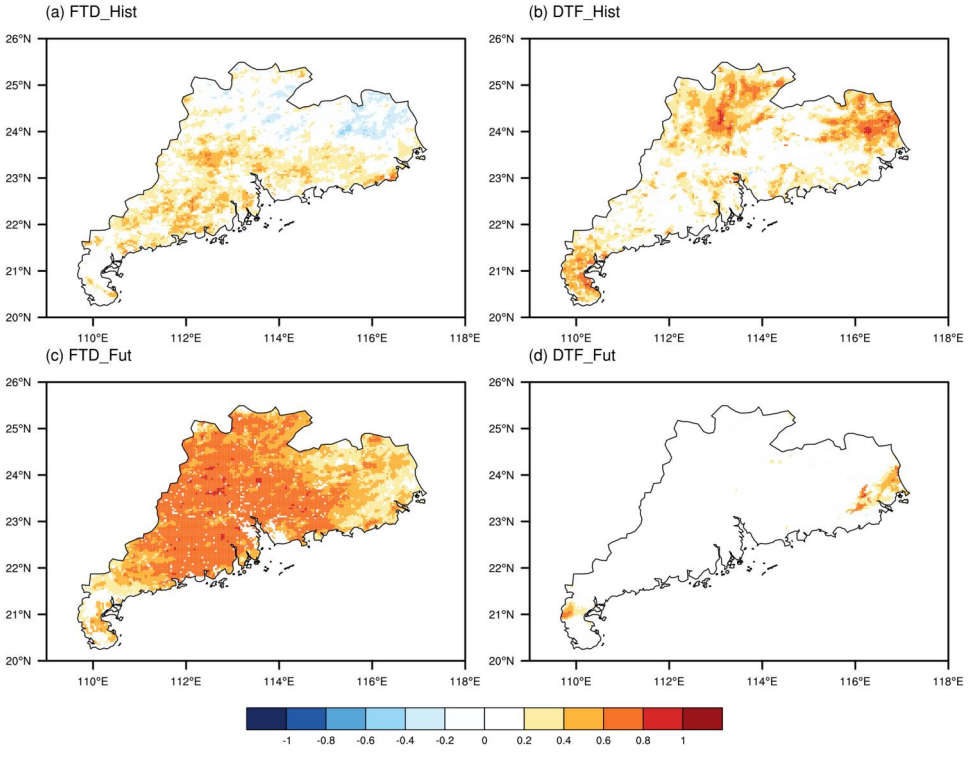

Figure 9. The map of the correlation between soil erosion and DFAA for two periods.

DTF events to FTD events. This transition renders the existing soil conservation measures inadequate, posing significant challenges for climate change adaptation and ecological protection in the region.

4. Discussion

This research investigates the impact of increasing spatial resolutions from 25 to 4 km on the simulation of extreme precipitation. The findings demonstrate that the CPM outperforms coarse-resolution climate models in reproducing erosive rainfall in the study area by effectively capturing convection processes. Additionally, the CPM shows significant improvements in simulating the heterogeneous distribution of rainfall, which plays a crucial role in the occurrence of DFAA events for pre-flood and post-flood seasons. Although the convection-permitting climate simulation provides detailed regional information, it still exhibits biases in simulated precipitation and its extremes. Certain limitations, such as the overemphasis on deep convective processes, inadequate local mixing, and unreliable large-scale forcing conditions, may hinder the CPM's effectiveness in some areas. However, for the period between April and September, which experiences the most drastic climate changes in Guangdong, the CPM performs notably better than coarse-resolution climate models in simulating extreme precipitation. Therefore, increasing the spatial resolution of the model is essential for improving the accuracy of erosive rainfall and extreme events, providing

a robust foundation for reliable simulation and analysis of soil erosion and its response to climate change.

The future period will witness a more heterogeneous distribution of precipitation, leading to an increased occurrence of DFAA events. Building upon previous studies that have demonstrated the viability of LDFAI in capturing DFAA events (Shi et al. 2021; Ren et al. 2023), we employ LDFAI to analyze the characteristics of DFAA events in Guangdong Province. Our findings reveal the dominance of FTD events within DFAA events. Notably, consistent with the research conducted by He et al. (2016) and Li et al. (2021), the eastern part of Guangdong experiences a higher frequency of DTF events, while the western part exhibits a greater occurrence of FTD events. Furthermore, in line with the investigations by Chen et al. (2020) and Qiao et al. (2022), our study illustrates that FTD events demonstrate an increasing trend under the influence of climate change, expanding toward the borders of Guangdong compared to the historical period. Additionally, both the frequency and intensity of extreme precipitation display an upward trajectory during the pre-flood season, while a decline is observed during the post-flood season. The escalating risk posed by these compound extreme events presents a significant challenge for soil and water conservation efforts. Therefore, it is of utmost importance that we proactively address these challenges by developing effective solutions and implementing appropriate responses to minimize the impact on our environment and communities.

The calculated historical average annual soil erosion rate in Guangdong, using the RUSLE model, is found to be 232 $t{\cdot}hm^{-2}{\cdot}a^{-1}$, which is similar to the findings of Gao et al. (2017). Consistent with the findings of Li et al. (2021), we anticipate that climate warming will further exacerbate soil loss through increased extreme events in the future. Our findings indicate a positive correlation between FTD events and soil erosion throughout most of Guangdong Province under the influence of climate change, rather than DTF events. Climate change has led to an increase in such extreme events which have a direct impact on soil erosion, exacerbating the degree of erosion. Soil erosion, in turn, results in the migration and alteration of soil organic carbon (Doetterl et al. 2016). The release and loss of organic carbon from the soil increase the concentration of greenhouse gases in the atmosphere (Yue et al. 2016; Van Oost and Six 2023), further intensifying the process of climate change. This interactive relationship forms a positive feedback loop, where climate change leads to an increase in extreme events (Zhang et al. 2016), which worsen soil erosion. Soil erosion, in turn, releases more organic carbon, exacerbating climate change, and subsequently impacting the occurrence and intensity of extreme events. This cycle contributes to further environmental issues and climate instability, emphasizing the importance of taking measures to mitigate climate change, protect soil, and implement sustainable land management practices.

5. Conclusion

This study provides valuable insights into the impact of increased spatial resolution on the simulation of extreme precipitation, soil erosion, and DFAA events in Guangdong Province. We investigate the interrelationship between soil erosion and

DFAA events for the first time, addressing previously neglected risks based on reliable outputs from the CPM. Our main findings can be summarized into three key points.

Firstly, the CPM outperforms coarse-resolution RCMs in reproducing erosive rainfall by effectively capturing convection processes. While RCMs provide detailed regional information, they exhibit large biases in simulating precipitation and its extremes. The CPM demonstrates significant improvements in simulating the heterogeneous distribution of rainfall, which is crucial for understanding DFAA events during pre-flood and post-flood seasons. Therefore, utilizing high-resolution models like CPM is essential for accurately simulating erosive rainfall and its impact on soil erosion and DFAA events.

Secondly, our research highlights that future periods will experience a more heterogeneous distribution of precipitation, resulting in an increased occurrence of DFAA events. FTD events exhibit an upward trend under the influence of climate change, expanding towards the borders of Guangdong compared to the historical period. Additionally, both the frequency and intensity of extreme precipitation show an increasing trajectory during the pre-flood season, while a decline is observed during the post-flood season. Climate warming will further contribute to soil loss through increased extreme events. During the historical period, the study area had an average soil erosion rate of 232 $t \cdot hm^{-2} \cdot a^{-1}$. Under the RCP8.5 scenario, soil loss increases by 26% compared to the historical period, with 73% of the area experiencing more severe soil erosion intensity.

Thirdly, our study reveals a positive correlation between FTD events and soil erosion throughout most of Guangdong Province, as opposed to DTF events. This correlation will be further amplified under RCP8.5, with an increase in the frequency of FTD events and a decrease in DTF events. This transition renders existing soil conservation measures inadequate, posing significant challenges for climate change adaptation and ecological protection in the region. Furthermore, climate change contributes to an increase in extreme events, such as DFAA, which exacerbate soil erosion. Soil erosion, in turn, releases more organic carbon, intensifying climate change and subsequently impacting the occurrence and intensity of extreme events.

Finally, we acknowledge that it is still challenging to study the physical effects of DFAA events on soil erosion. In this article, the effects of DFAA events on soil erosion have been studied by simply linking the corresponding relationships using the correlation coefficients, and the physical mechanisms have not been studied in depth. Thereafter, the study of soil erosion during pre-flood and post-flood periods can be considered separately.

Acknowledgments

We acknowledge and thank the climate modeling groups in the Coordinated Regional Climate Downscaling Experiment and Coupled Model Intercomparison Project for generating their model outputs and making them available.

Disclosure statement

No potential conflict of interest was reported by the author(s).

Funding

This study was supported by the National Natural Science Foundation of China (Grant No. 42301021) and the Guangdong Natural Science Foundation (Grant No. 2023A1515012046).

References

AghaKouchak A, Cheng L, Mazdiyasni O, Farahmand A. 2014. Global warming and changes in risk of concurrent climate extremes: insights from the 2014 California drought. Geophys Res Lett. 41(24):8847–8852. doi: 10.1002/2014GL062308.

AghaKouchak A, Chiang F, Huning LS, Love CA, Mallakpour I, Mazdiyasni O, Moftakhari H, Papalexiou SM, Ragno E, Sadegh M. 2020. Climate extremes and compound hazards in a warming world. Annu Rev Earth Planet Sci. 48(1):519–548. doi: 10.1146/annurev-earth-071719-055228.

Amundson R, Berhe AA, Hopmans JW, Olson C, Sztein AE, Sparks DL. 2015. Soil and human security in the 21st century. Science. 348(6235):1261071. doi: 10.1126/science.1261071.

Ascott MJ, Christelis V, Lapworth DJ, Macdonald DMJ, Tindimugaya C, Iragena A, Finney D, Fitzpatrick R, Marsham JH, Rowell DP. 2023. On the application of rainfall projections from a convection-permitting climate model to lumped catchment models. J Hydrol. 617: 129097. doi: 10.1016/j.jhydrol.2023.129097.

Azari M, Oliaye A, Nearing MA. 2021. Expected climate change impacts on rainfall erosivity over Iran based on CMIP5 climate models. J Hydrol. 593:125826. doi: 10.1016/j.jhydrol.2020.125826.

Ban N, Rajczak J, Schmidli J, Schär C. 2020. Analysis of alpine precipitation extremes using generalized extreme value theory in convection-resolving climate simulations. Clim Dyn. 55(1–2):61–75. doi: 10.1007/s00382-018-4339-4.

Ban N, Schmidli J, Schär C. 2014. Evaluation of the convection-resolving regional climate modeling approach in decade-long simulations. J Geophys Res Atmos. 119(13):7889–7907. doi: 10.1002/2014JD021478.

Basheer S, Wang X, Farooque AA, Nawaz RA, Pang T, Neokye EO. 2024. A review of greenhouse gas emissions from agricultural soil. Sustainability. 16(11):4789.). doi: 10.3390/su16114789.

Bi W, Li M, Weng B, Yan D, Dong Z, Feng J, Wang H. 2023. Drought-flood abrupt alteration events over China. Sci Total Environ. 875:162529. doi: 10.1016/j.scitotenv.2023.162529.

Bi W, Weng B, Yan D, Wang M, Wang H, Jing L, Yan S. 2022. Soil phosphorus loss increases under drought-flood abrupt alternation in summer maize planting areas. Agric Water Manage. 262:107426. doi: 10.1016/j.agwat.2021.107426.

Borrelli P, Robinson DA, Fleischer LR, Lugato E, Ballabio C, Alewell C, Meusburger K, Modugno S, Schütt B, Ferro V, et al. 2017. An assessment of the global impact of 21st century land use change on soil erosion. Nat Commun. 8(1):2013. doi: 10.1038/s41467-017-02142-7.

Borrelli P, Robinson DA, Panagos P, Lugato E, Yang JE, Alewell C, Wuepper D, Montanarella L, Ballabio C. 2020. Land use and climate change impacts on global soil erosion by water (2015–2070). Proc Natl Acad Sci U S A. 117(36):21994–22001. doi: 10.1073/pnas.2001403117.

Cai G, Chen S, Liu Y, Sun H, Chen C, Gui D, Yan D. 2020. Using multiple indexes to analyze temporal and spatial patterns of precipitation and drought in Xinjiang, China. Theor Appl Climatol. 142(1–2):177–190. doi: 10.1007/s00704-020-03302-4.

Chan SC, Kendon EJ, Fowler HJ, Blenkinsop S, Roberts NM, Ferro CAT. 2014. The value of high-resolution met office regional climate models in the simulation of multihourly precipitation extremes. J Climate. 27(16):6155–6174. doi: 10.1175/JCLI-D-13-00723.1.

Chen H, Wang S. 2022. Accelerated transition between dry and wet periods in a warming climate. Geophys Res Lett. 49(19):e2022G–e99766G. doi: 10.1029/2022GL099766.

Chen H, Wang S, Zhu J, Wang D. 2023. Projected changes in the pattern of spatially compounding drought and pluvial events over Eastern China under a warming climate. Earth's Future. 11(5):e2022E–e3397E. doi: 10.1029/2022EF003397.
Chen H, Wang S, Zhu J, Zhang B. 2020. Projected changes in abrupt shifts between dry and wet extremes Over China through an ensemble of regional climate model simulations. JGR Atmospheres. 125(23):e2020J–e33894J. doi: 10.1029/2020JD033894.
Coles S. 2001. An introduction to statistical modeling of extreme values. London: Springer. doi: 10.1007/978-1-4471-3675-0.
Dai A, Giorgi F, Trenberth KE. 1999. Observed and model-simulated diurnal cycles of precipitation over the contiguous United States. J Geophys Res. 104(D6):6377–6402. doi: 10.1029/98JD02720.
de Vries F, Lau J, Hawkes C, Semchenko M. 2023. Plant–soil feedback under drought: Does history shape the future? Trends Ecol Evol. 38(8):708–718. doi: 10.1016/j.tree.2023.03.001.
Doetterl S, Berhe AA, Nadeu E, Wang Z, Sommer M, Fiener P. 2016. Erosion, deposition and soil carbon: a review of process-level controls, experimental tools, and models to address C cycling in dynamic landscapes. Earth Sci Rev. 154:102–122. doi: 10.1016/j.earscirev.2015.12.005.
Du Z, Wang J, An H, Zhang H, Chen G. 2023. Responses of soil seed banks to drought on a global scale. Sci Total Environ. 864:161142. doi: 10.1016/j.scitotenv.2022.161142.
Elnashar A, Zeng H, Wu B, Fenta AA, Nabil M, Duerler R. 2021. Soil erosion assessment in the Blue Nile Basin driven by a novel RUSLE-GEE framework. Sci Total Environ. 793:148466. doi: 10.1016/j.scitotenv.2021.148466.
Fosser G, Khodayar S, Berg P. 2015. The benefit of convection permitting climate model simulations in the representation of convective precipitation. Clim Dyn. 44(1-2):45–60. doi: 10.1007/s00382-014-2242-1.
Ganasri BP, Ramesh H. 2016. Assessment of soil erosion by RUSLE model using remote sensing and GIS: a case study of Nethravathi Basin. Geosci Front. 7(6):953–961. doi: 10.1016/j.gsf.2015.10.007.
Gao F, Wang Y, Yang J. 2017. Assessing soil erosion using the USLE model and MODIS data in Guangdong, China. IOP Conf Ser: earth Environ Sci. 74(1):012007. doi: 10.1088/1755-1315/74/1/012007.
Gao X, Xu Y, Zhao Z, Pal JS, Giorgi F. 2006. On the role of resolution and topography in the simulation of East Asia precipitation. Theor Appl Climatol. 86(1-4):173–185. doi: 10.1007/s00704-005-0214-4.
Ghosal K, Das Bhattacharya S. 2020. A review of the RUSLE model. J Indian Soc Remote Sens. 48(4):689–707. doi: 10.1007/s12524-019-01097-0.
Guo Z, Fang J, Sun X, Yang Y, Tang J. 2019. Sensitivity of summer precipitation simulation to microphysics parameterization Over Eastern China: convection-permitting regional climate simulation. JGR Atmospheres. 124(16):9183–9204. doi: 10.1029/2019JD030295.
Guo J, Liang X, Wang X, Fan Y, Liu L. 2023. Potential benefits of limiting global warming for the mitigation of temperature extremes in China. Npj Clim Atmos Sci. 6(1):106. doi: 10.1038/s41612-023-00412-4.
He Y, Hu X, Xu W, Fang J, Shi P. 2022. Increased probability and severity of compound dry and hot growing seasons over the world's major croplands. Sci Total Environ. 824:153885. doi: 10.1016/j.scitotenv.2022.153885.
He H, Liao X, Lu H, Chen S. 2016. Features of long-cycle drought-flood abrupt alternation in South China during summer in 1961-2014. Acta Geographica Sinica. 71(01):130–141. doi: 10.11821/dlxb201601010.
Horton DE, Johnson NC, Singh D, Swain DL, Rajaratnam B, Diffenbaugh NS. 2015. Contribution of changes in atmospheric circulation patterns to extreme temperature trends. Nature. 522(7557):465–469. doi: 10.1038/nature14550.
IPCC. 2021. Climate change 2021: the physical science basis. Contribution of Working Group I to the Sixth Assessment Report of the Intergovernmental Panel on Climate Change. In V. Masson-Delmotte, P. Zhai, A. Pirani, S. L. Connors, C. Péan, S. Berger, N. Caud, Y. Chen,

L. Goldfarb, M. I. Gomis, et al., editors. Cambridge: Cambridge University Press; p. 2061–2086. doi: 10.1017/9781009157896.015.
Jaafari A, Janizadeh S, Abdo HG, Mafi-Gholami D, Adeli B. 2022. Understanding land degradation induced by gully erosion from the perspective of different geoenvironmental factors. J Environ Manage. 315:115181. doi: 10.1016/j.jenvman.2022.115181.
Knijff J, Jones R, Montanarella L. 2000. Soil erosion risk assessment in Europe.
Liao Y, Li D, Zhuo M, Wei G, Xie Z, Guo T, Li J. 2014. Spatio-temporal variation and tendency of rainfall in Guangdong province during past 50 years. Ecol Environ Sci. 23(2):223–228. doi: 10.16258/j.cnki.1674-5906.2014.02.003.
Li Z, Fang H. 2016. Impacts of climate change on water erosion: a review. Earth Sci Rev. 163: 94–117. doi: 10.1016/j.earscirev.2016.10.004.
Li D, Qi Y, Zhou T. 2021. Changes in rainfall erosivity over mainland China under stabilized 1.5 °C and 2 °C warming futures. J Hydrol. 603:126996. doi: 10.1016/j.jhydrol.2021.126996.
Liu Y, Chen S, Sun H, Gui D, Xue J, Lei J, Zeng X, Lv G. 2019. Do long-term precipitation variations and dry-wet conditions exist in arid areas? A case study from China. Quat Int. 519:3–9. doi: 10.1016/j.quaint.2019.01.034.
Liu H, Liu X, Liu C, Yun Y. 2023. High-resolution regional climate modeling of warm-season precipitation over the Tibetan Plateau: impact of grid spacing and convective parameterization. Atmos Res. 281:106498. doi: 10.1016/j.atmosres.2022.106498.
Liu B, Xie Y, Li Z, Liang Y, Zhang W, Fu S, Yin S, Wei X, Zhang K, Wang Z, et al. 2020. The assessment of soil loss by water erosion in China. Intern Soil Water Conserv Res. 8(4):430–439. doi: 10.1016/j.iswcr.2020.07.002.
Li S, Wang Z, Lai C, Lin G. 2020. Quantitative assessment of the relative impacts of climate change and human activity on flood susceptibility based on a cloud model. J Hydrol. 588: 125051. doi: 10.1016/j.jhydrol.2020.125051.
Li S, Zhong D, Wu Y, Zeng S, Ye X. 2021. Spatial-temporal evolution characteristic of drought-flood abrupt alternation during main flood season in northeast Guangdong. Guangdong Water Resources and Hydropower (04), 79–83.
Lucas-Picher P, Laprise R, Winger K. 2017. Evidence of added value in North American regional climate model hindcast simulations using ever-increasing horizontal resolutions. Clim Dyn. 48(7-8):2611–2633. doi: 10.1007/s00382-016-3227-z.
Ma Y, Yang Y, Wang C. 2019. How essential is the balance between large and small-scale features to reproduce precipitation during a sudden sharp turn from drought to flood. Clim Dyn. 52(7–8):5013–5029. doi: 10.1007/s00382-018-4445-3.
Masroor M, Sajjad H, Rehman S, Singh R, Hibjur Rahaman M, Sahana M, Ahmed R, Avtar R. 2022. Analysing the relationship between drought and soil erosion using vegetation health index and RUSLE models in Godavari middle sub-basin, India. Geosci Front. 13(2):101312. doi: 10.1016/j.gsf.2021.101312.
Nearing MA, Pruski FF, O'Neal MR. 2004. Expected climate change impacts on soil erosion rates: a review. J Soil Water Conserv. 59:43–50.
Papalexiou SM, Montanari A. 2019. Global and regional increase of precipitation extremes under global warming. Water Resour Res. 55(6):4901–4914. doi: 10.1029/2018WR024067.
Peng S. 2020. 1-km Monthly precipitation dataset for China (1901–2021): a big earth data platform for three poles.
Peng S, Ding Y, Liu W, Li Z. 2019. 1-km Monthly temperature and precipitation dataset for China from 1901 to 2017. Earth Syst Sci Data. 11(4):1931–1946. doi: 10.5194/essd-11-1931-2019.
Peng X, Horn R, Smucker A. 2007. Pore shrinkage dependency of inorganic and organic soils on wetting and drying cycles. Soil Science Soc of Amer J. 71(4):1095–1104. doi: 10.2136/sssaj2006.0156.
Pfahl S, O Gorman PA, Fischer EM. 2017. Understanding the regional pattern of projected future changes in extreme precipitation. Nature Clim Change. 7(6):423–427. doi: 10.1038/nclimate3287.

Phinzi K, Ngetar NS. 2019. The assessment of water-borne erosion at catchment level using GIS-based RUSLE and remote sensing: a review. Intern Soil Water Conserv Res. 7(1):27–46. doi: 10.1016/j.iswcr.2018.12.002.

Polade SD, Gershunov A, Cayan DR, Dettinger MD, Pierce DW. 2017. Precipitation in a warming world: Assessing projected hydro-climate changes in California and other Mediterranean climate regions. Sci Rep. 7(1):10783. doi: 10.1038/s41598-017-11285-y.

Prein AF, Langhans W, Fosser G, Ferrone A, Ban N, Goergen K, Keller M, Tölle M, Gutjahr O, Feser F, et al. 2015. A review on regional convection-permitting climate modeling: demonstrations, prospects, and challenges. Rev Geophys. 53(2):323–361. doi: 10.1002/2014RG000475.

Qiao F, Liang X. 2015. Effects of cumulus parameterizations on predictions of summer flood in the Central United States. Clim Dyn. 45(3–4):727–744. doi: 10.1007/s00382-014-2301-7.

Qiao Y, Xu W, Wu D, Meng C, Qin L, Li Z, Zhang X. 2022. Changes in the spatiotemporal patterns of dry/wet abrupt alternation frequency, duration, and severity in Mainland China, 1980–2019. Sci Total Environ. 838(Pt 3):156521. doi: 10.1016/j.scitotenv.2022.156521.

Ren J, Wang W, Wei J, Li H, Li X, Liu G, Chen Y, Ye S. 2023. Evolution and prediction of drought-flood abrupt alternation events in Huang-Huai-Hai River Basin, China. Sci Total Environ. 869:161707. doi: 10.1016/j.scitotenv.2023.161707.

Schulze ED, Freibauer A. 2005. Carbon unlocked from soils. Nature. 437(7056):205–206. doi: 10.1038/437205a.

Shi W, Huang S, Liu D, Huang Q, Han Z, Leng G, Wang H, Liang H, Li P, Wei X. 2021. Drought-flood abrupt alternation dynamics and their potential driving forces in a changing environment. J Hydrol. 597:126179. doi: 10.1016/j.jhydrol.2021.126179.

Shmilovitz Y, Marra F, Wei H, Argaman E, Nearing M, Goodrich D, Assouline S, Morin E. 2021. Frequency analysis of storm-scale soil erosion and characterization of extreme erosive events by linking the DWEPP model and a stochastic rainfall generator. Sci Total Environ. 787:147609. doi: 10.1016/j.scitotenv.2021.147609.

Shu C, Gaur A, Wang LL, Bartko M, Laouadi A, Ji L, Lacasse M. 2022. Added value of convection permitting climate modelling in urban overheating assessments. Build Environ. 207: 108415. doi: 10.1016/j.buildenv.2021.108415.

Tang Q, Xu Y, Bennett SJ, Li Y. 2015. Assessment of soil erosion using RUSLE and GIS: a case study of the Yangou watershed in the Loess Plateau, China. Environ Earth Sci. 73(4): 1715–1724. doi: 10.1007/s12665-014-3523-z.

Thomas J, Joseph S, Thrivikramji KP. 2018. Assessment of soil erosion in a tropical mountain river basin of the southern Western Ghats, India using RUSLE and GIS. Geosci Front. 9(3): 893–906. doi: 10.1016/j.gsf.2017.05.011.

Tian P, Zhu Z, Yue Q, He Y, Zhang Z, Hao F, Guo W, Chen L, Liu M. 2021. Soil erosion assessment by RUSLE with improved P factor and its validation: case study on mountainous and hilly areas of Hubei Province, China. Intern Soil Water Conserv Res. 9(3):433–444. doi: 10.1016/j.iswcr.2021.04.007.

Van Oost K, Six J. 2023. Reconciling the paradox of soil organic carbon erosion by water. Biogeosciences. 20(3):635–646. doi: 10.5194/bg-20-635-2023.

Wang R, Li L, Gentine P, Zhang Y, Chen J, Chen X, Chen L, Ning L, Yuan L, Lü G. 2022. Recent increase in the observation-derived land evapotranspiration due to global warming. Environ Res Lett. 17(2):024020. doi: 10.1088/1748-9326/ac4291.

Weber T, Bowyer P, Rechid D, Pfeifer S, Raffaele F, Remedio AR, Teichmann C, Jacob D. 2020. Analysis of compound climate extremes and exposed population in Africa under two different emission scenarios. Earth's Future. 8(9):e1473E–e2019E. doi: 10.1029/2019EF001473.

Williams JR. 1990. EPIC-erosion/productivity impact calculator: 1. Model documentation. Technical Bulletin - United States Department of Agriculture. 4(4):206–207.

Wu Z, Li J, He J, Jiang Z. 2006. Occurrence of droughts and floods during the normal summer monsoons in the mid- and lower reaches of the Yangtze River. Geophys Res Lett. 33(5) doi: 10.1029/2005GL024487.

Xie Y, Yin S, Liu B, Nearing MA, Zhao Y. 2016. Models for estimating daily rainfall erosivity in China. J Hydrol. 535:547–558. doi: 10.1016/j.jhydrol.2016.02.020.

Xue J, Lyu D, Wang D, Wang Y, Yin D, Zhao Z, Mu Z. 2018. Assessment of soil erosion dynamics using the GIS-based RUSLE model: a case study of Wangjiagou watershed from the three gorges reservoir region, Southwestern China water. Water. 10(12):1817. doi: 10.3390/w10121817.

Yu X, Wang Y, Yu S, Kang Z. 2019. Synchronous droughts and floods in the Southern Chinese Loess Plateau since 1646 CE in phase with decadal solar activities. Global Planet Change. 183:103033. doi: 10.1016/j.gloplacha.2019.103033.

Yue Y, Ni J, Ciais P, Piao S, Wang T, Huang M, Borthwick AGL, Li T, Wang Y, Chappell A, et al. 2016. Lateral transport of soil carbon and land – atmosphere CO2 flux induced by water erosion in China. Proc Natl Acad Sci U S A. 113(24):6617–6622. doi: 10.1073/pnas.1523358113.

Zhang Y, Chao Y, Fan R, Ren F, Qi B, Ji K, Xu B. 2021b. Spatial-temporal trends of rainfall erosivity and its implication for sustainable agriculture in the Wei River Basin of China. Agric Water Manage. 245(C):106557. doi: 10.1016/j.agwat.2020.106557.

Zhang B, He C, Burnham M, Zhang L. 2016. Evaluating the coupling effects of climate aridity and vegetation restoration on soil erosion over the Loess Plateau in China. Sci Total Environ. 539:436–449. doi: 10.1016/j.scitotenv.2015.08.132.

Zhang W, Luo M, Gao S, Chen W, Hari V, Khouakhi A. 2021a. Compound hydrometeorological extremes: drivers, mechanisms and methods. Front Earth Sci. 9:673495. doi: 10.3389/feart.2021.673495.

Zhang ZB, Peng X, Wang LL, Zhao QG, Lin H. 2013. Temporal changes in shrinkage behavior of two paddy soils under alternative flooding and drying cycles and its consequence on percolation. Geoderma. 192:12–20. doi: 10.1016/j.geoderma.2012.08.009.

Zhang Y, You Q, Ullah S, Chen C, Shen L, Liu Z. 2023. Substantial increase in abrupt shifts between drought and flood events in China based on observations and model simulations. Sci Total Environ. 876:162822. doi: 10.1016/j.scitotenv.2023.162822.

Zhu R, Wu F, Zhou S, Hu T, Huang J, Gao Y. 2020. Cumulative effects of drought–flood abrupt alternation on the photosynthetic characteristics of rice. Environ Exp Bot. 169:103901. doi: 10.1016/j.envexpbot.2019.103901.

Zscheischler J, Martius O, Westra S, Bevacqua E, Raymond C, Horton RM, van den Hurk B, AghaKouchak A, Jézéquel A, Mahecha MD, et al. 2020. A typology of compound weather and climate events. Nat Rev Earth Environ. 1(7):333–347. doi: 10.1038/s43017-020-0060-z.

Zscheischler J, Seneviratne SI. 2017. Dependence of drivers affects risks associated with compound events. Sci Adv. 3(6):e1700263. doi: 10.1126/sciadv.1700263.